ACS central science

http://pubs.acs.org/journal/acscii

Research Article

Phylogeny-Informed Synthetic Biology Reveals Unprecedented Structural Novelty in Type V Glycopeptide Antibiotics

Min Xu, Wenliang Wang, Nicholas Waglechner, Elizabeth J. Culp, Allison K. Guitor, and Gerard D. Wright*

Cite This: *ACS Cent. Sci.* 2022, 8, 615−626

Read Online

ACCESS | Metrics & More | Article Recommendations | Supporting Information

ABSTRACT: The rise and dissemination of glycopeptide antibiotic (GPA)-resistant pathogens in healthcare settings fuel efforts to discover GPAs that can overcome resistance. Members of the type V subclass of GPAs can evade common GPA resistance mechanisms and offer promise as new drug leads. We characterize five new type V GPAs—rimomycin-A/B/C and misaugamycin-A/B—discovered through a phylogeny-guided genome mining strategy coupled with heterologous production using our GPAHex synthetic biology platform. Rimomycin is a heptapeptide similar to kistamicin but includes an *N*-methyl-tyrosine at amino acid 6 (AA6) and substitutes 4-hydroxyphenylglycine for tyrosine and 3,5-dihydroxyphenylglycine at positions AA1 and AA3. Misaugamycin is characterized by an unprecedented N−C cross-link between AA2 and AA4 and unique N-terminal acylation by malonyl (misaugamycin-A) or 2-sulfoacetyl (misaugamycin-B) groups. We demonstrate that rimomycin-A/B/C and misaugamycin-A/B are potent antibiotics with activity against GPA-resistant clinical isolates and that the mode of action is consistent with the inhibition of cell division by the evasion of autolysin activity. These discoveries expand the chemical diversity of the type V GPAs, offer new chemical scaffolds for drug development, and demonstrate the application of the GPAHex platform in mining GPA chemical "dark matter".

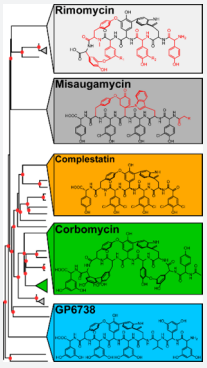

INTRODUCTION

Glycopeptide antibiotics (GPAs) such as vancomycin and teicoplanin are natural product drugs that are vital for treating serious infections caused by Gram-positive pathogens, particularly multi-drug-resistant enterococci and *Staphylococcus aureus*.[1] GPAs have gradually lost their efficacy against life-threatening pathogens because of the development of resistance.[2] Most GPAs inhibit bacterial growth through binding to the D-alanyl-D-alanine (D-Ala-D-Ala) terminus of the peptidoglycan (PG) stem peptide, thereby blocking the cross-linking and extension of the polymer.[3] Replacing the terminal D-Ala-D-Ala dipeptide by D-Ala-D-lactate (D-Ala-D-Lac) through the expression of *vanHAX* resistance genes is the dominant resistance mechanism for GPAs in environmental and clinical settings where it is expressed in enterococci.[4−6] On the other hand, thickening the cell wall in *Staphylococcus* can also provide redundant D-Ala-D-Ala termini that can neutralize GPAs, resulting in intermediate resistance to vancomycin.[7,8] To address the growing resistance challenge, three D-Ala-D-Ala-binding second-generation semisynthetic GPAs (telavancin, dalbavancin, and oritavancin) were introduced to the market over the past decade.[9−11] However, the foreseeable development of resistance to these second-generation GPAs requires continued effort to discover and develop more effective GPAs and other Gram-positive-directed antibiotics.[12]

GPAs are grouped into five (I−V) structural subtypes.[13] Type I GPAs such as vancomycin have aliphatic amino acids at AA1 and AA3. Type II−IV GPAs are composed entirely of aromatic amino acids. The chemical structures of GPAs are further diversified by postaglycone modifications such as methylation, glycosylation, sulfation, and acylation.[14] Type I−IV GPAs bind D-Ala-D-Ala as described above to achieve their antibacterial impact. On the other hand, type V GPAs such as complestatin and kistamicin are characterized by the presence of a D-E biaryl ring system composed of tryptophan (Trp) and a central 4-hydroxyphenylglycine (Hpg), and corbomycin[15] and GP6738[16] possess a nonapeptide scaffold distinct from that of the canonical type I−IV GPA heptapeptides (Figure 1A). Unlike type I−IV GPAs, type V GPAs lack postaglycone modifications including glycosylation. We recently reported that type V GPAs, including complestatin, corbomycin, and GP6738, exhibit a different mode of action (MOA) than D-Ala-D-Ala-binding type I−IV GPAs.[15,16] Instead, type V GPAs bind PG and impair bacterial growth through the indirect inhibition of autolysins, which are essential PG hydrolases required to remodel the cell wall during elongation and division.[15] Consequently, type V GPAs overcome the D-Ala-D-Lac GPA resistance and exhibit potent antibacterial activity against vancomycin-resistant enterococci

Received: November 10, 2021
Published: April 27, 2022

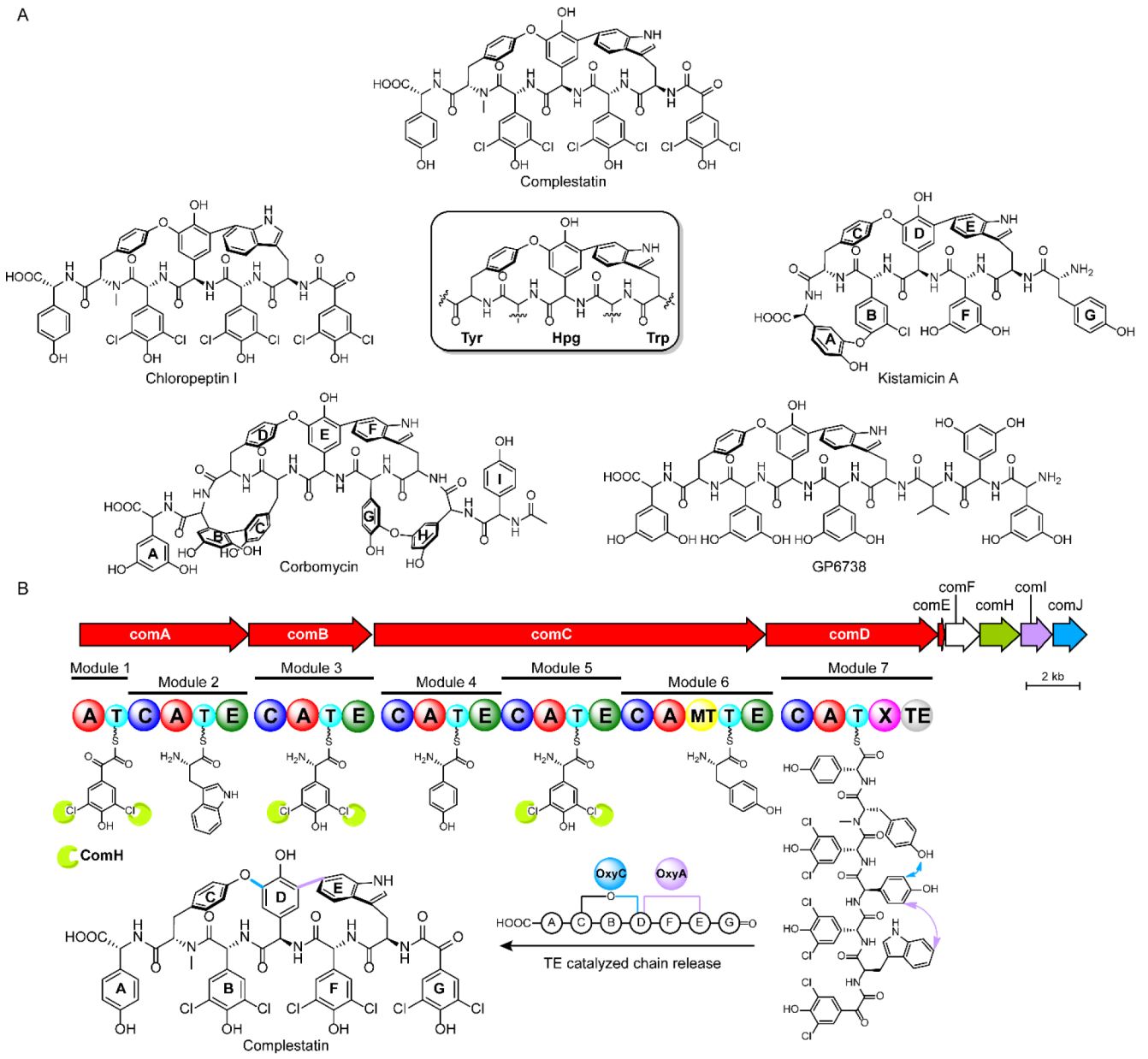

Figure 1. Structures of type V GPAs and the schematic biosynthetic pathway of complestatin. (A) Chemical structures of type V GPAs. Type V GPAs are classified by the presence of the conserved central Trp-Hpg-(m)Tyr cross-linked structural motif. Kistamicin has an extra A−*O*−B ring, and corbomycin has two extra B−C and G−*O*−H ring structures. Most GPAs are heptapeptides; however, corbomycin and GP6738 represent the only two known nonapeptide GPAs. (B) Complestatin biosynthetic pathway as an example of GPA biosynthesis. The core NRPS scaffold genes (*comA-comD*), MbtH gene (*comE*), Na^+/H^+ antiporter gene (*comF*), halogenase gene (*comH*), and P450 monooxygenase genes (*comI-comJ*) are shown. NRPS domains are labeled as A, adenylation; C, condensation; T, thiolation or peptidyl carrier protein; E, epimerization; MT, methyltransferase; X, Oxy-recruting domain; and TE, thioesterase. The halogenation catalyzed by ComH takes place when the amino acid building block is tethered to the T domain. The characteristic ring cross-linking reactions are performed by specific Oxy proteins as shown. Numbering of the rings on the GPA scaffolds is shown in bold font.

(VRE). Therefore, type V GPAs offer a promising new group of antibiotics for further discovery and development.

GPAs are synthesized by multimodular nonribosomal peptide synthetase (NRPS) systems[17−20] (Figure 1B). The genes encoding the biosynthetic machinery of GPAs and other NPs are clustered in the chromosome in biosynthetic gene clusters (BGC). GPA BGCs possess genes required for peptide assembly, the amino acid precursor supply, scaffold cross-linking and modification, resistance, regulation, and transport.[14] In addition to common amino acids, GPAs include several nonproteinogenic amino acid building blocks, including Hpg, 3,5-dihydroxyphenylglycine (Dpg), and β-hydroxytyrosine (βHT). The NRPS mega-enzymes assemble the peptide scaffold through collaboration among the adenylation (A), thiolation/peptidyl carrier protein (T/PCP), and condensation (C) domains. Amino acid building blocks are recognized and activated by the A domains and then loaded onto the adjacent T domain, which is then condensed to the downstream T-tethered amino acid residue via an amide bond by the following C domain. During the extension of the peptide chain, epimerization (E) domains and the methyltransferase (MT) domain may also be involved to alter the L-amino acid to the D-

https://doi.org/10.1021/acscentsci.1c01389
ACS Cent. Sci. 2022, 8, 615−626

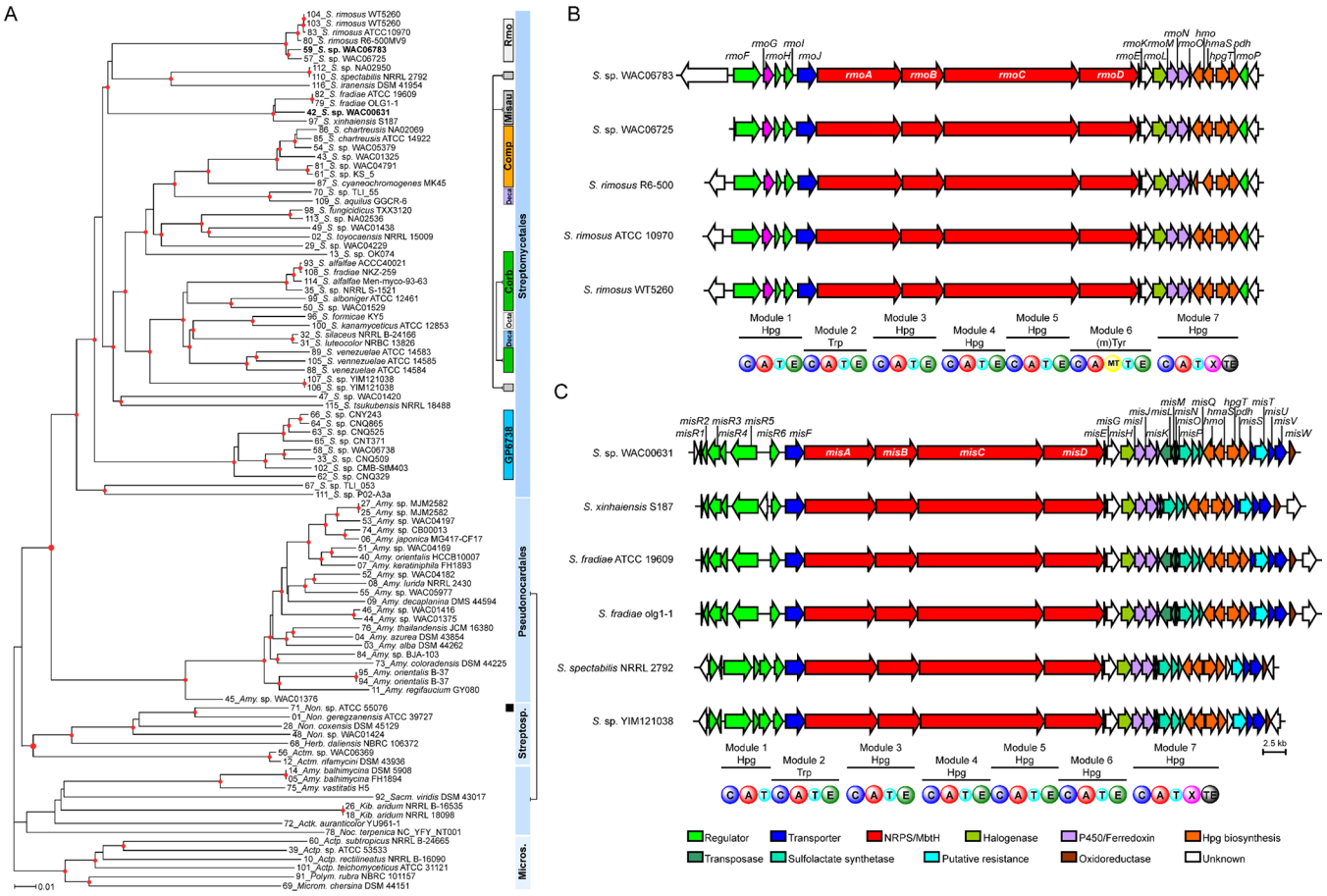

Figure 2. *In silico* analysis of the GPA BGCs. (A) MinHash distance phylogeny computed with a mashtree. Nodes with bootstrap support 80 and above are indicated by red circles. BGC numbers (Supporting Information) identified from each actinobacterium are also used to label each strain. Most type V GPA BGCs are found in *Streptomyces* and are grouped on the top half of the tree. *Streptomyces* strains are labeled with different squares according to the type V GPA BGCs they possess: orange (Comp, complestatin), green (Corb, corbomycin), azure (GP6738), light gray (Rmo, rimomycin), dark gray (Misau, misaugamycin), light purple (Deca, decapeptide type V GPA), white (Octa, octapeptide type V GPA), and light blue (Deca, corbomycin-like decapeptide type V GPA). The black square represents kistamicin BGC. Corbomycin BGC containing strains split into two subclades and misaugamycin BGC containing strains are divided into three subclades in the tree. Class names are abbreviated as *Streptosp.* (*Streptosporangiales*) and *Micros.* (*Micromonosporales*). Strains from the class of *Pseudonorcardales* form two subclades in the tree. Species names are abbreviated as *S.* (*Streptomyces*), *Amy.* (*Amycolatopsis*), *Non.* (*Nonomuraea*), *Herb.* (*Herbidospora*), *Actp.* (*Actinoplanes*), *Polym.* (*Polymorphospora*), *Microm.* (*Micromonospora*), *Actm.* (*Actinomadura*), *Kib.* (*Kibdellosporangium*), *Sacm.* (*Saccharomonospora*), *Actk.* (*Actinokineospora*), and *Noc.* (*Nocardia*). (B) Gene organization of rimomycin-related BGCs. Rimomycin BGCs show identical organization across the five *Streptomyces* strains. The domain organization of the NRPS assembly line is shown. Hpg biosynthetic genes are labeled as *hmo*, 4-hydroxymandelate oxidase; *hmaS*, 4-hydroxymandelate synthase; *hpgT*, 4-hydroxyphenylglycine transaminase; and *pdh*, prephenate dehydrogenase. Predicted amino acid building blocks loaded by the adenylation domains are shown. (C) Gene organization of misaugamycin-related BGCs. Misaugamycin BGCs show almost identical organization across the six *Streptomyces* strains except for the presence of two additional putative transposase genes (*misL* and *misM*) in WAC00631, *S. fradiae* ATCC 19609, and *S. fradiae* olg 1-1. BGCs of the other type V GPAs are shown in Figures S1−S5. NRPS domains are labeled as in Figure 1B.

configuration and install *N*-methyl groups 6. The chlorination of T-tethered amino acid residues and the β-hydroxylation of T-tethered tyrosine can also occur during the elongation process.[21−23] Multiple rounds of similar elongation steps result in the linear peptide scaffold of GPAs. Subsequently, the T-tethered GPA peptide scaffolds are cross-linked through sequential oxidative cyclization catalyzed by the P450 monooxygenases (OxyB > (OxyE) > OxyA > OxyC in type I−IV GPA biosynthesis[24−27]) to generate the rigid 3D structure that is characteristic of GPAs. The Oxy proteins are recruited by a conserved penultimate Oxy-recruiting domain, X-domain, to catalyze the oxidative cyclization.[28] One Oxy protein is typically responsible for the installation of one cross-link in GPA biosynthesis; however, OxyC from the kistamicin BGC was recently shown to perform dual oxidative cyclization in kistamicin biosynthesis.[20] OxyC from the corbomycin BGC is also believed to mediate dual oxidative cyclization in corbomycin biosynthesis,[15] suggesting that the Oxy proteins may represent a new diversification node for the generation of novel GPAs. The cross-linked GPA scaffolds are then released from the NRPS assembly line by terminal thioesterase (TE) domain-catalyzed hydrolysis. Subsequently, methylation, sulfation, glycosylation, and acylation may follow to further diversify the GPA scaffolds.

Our identification of new type V GPAs used a phylogenomic approach based on the analysis of the antibiotic BGCs, a strategy that revealed dozens of novel GPA BGCs.[29] This GPA reservoir has not been explored mainly because of the "cryptic/silent" nature of the clusters, where either the organisms produce the compounds in a low yield or often do not express them at all under laboratory conditions. To access this untapped GPA chemical "dark matter", we developed the GPAHex (glycopep-

https://doi.org/10.1021/acscentsci.1c01389
ACS Cent. Sci. 2022, 8, 615−626

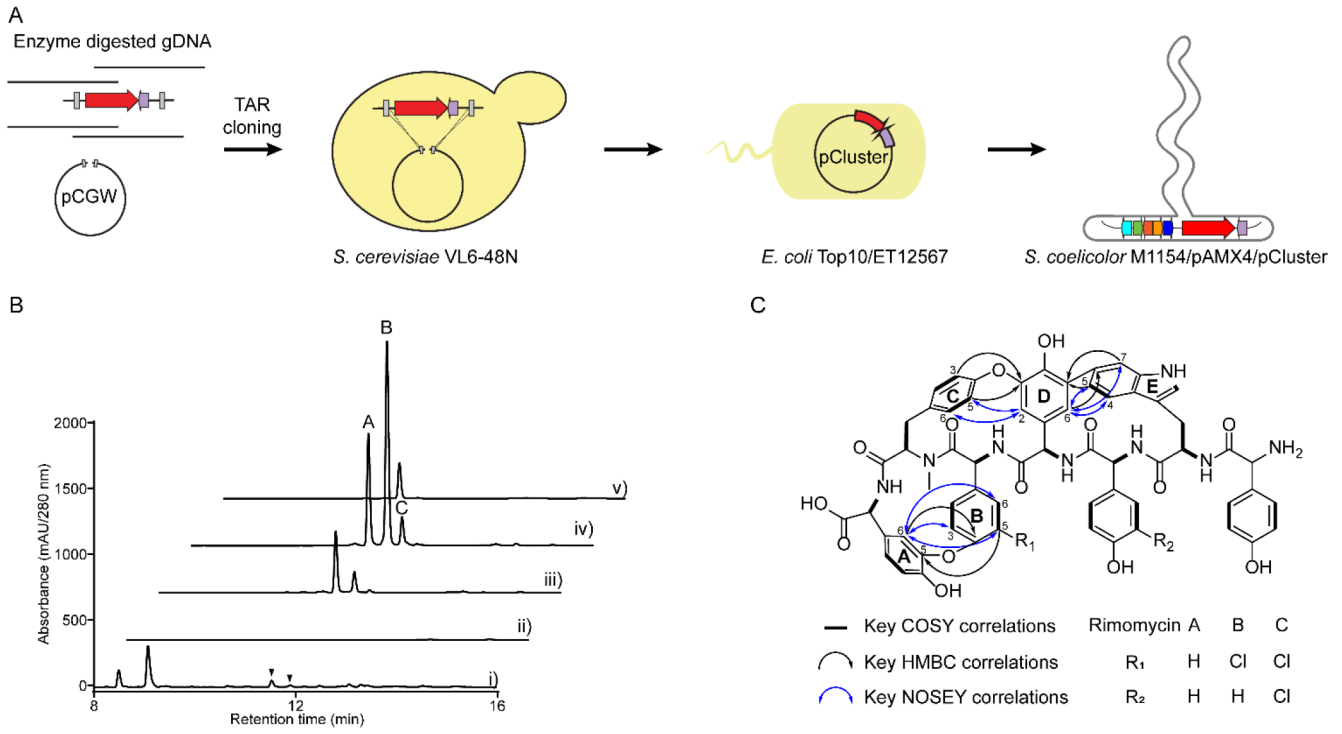

Figure 3. Discovery of rimomycin from WAC06783 using GPAHex. (A) General workflow of GPAHex for discovering GPAs. GPA BGCs of interest are captured using TAR in yeast, followed by expression in the GPAHex chassis strain *S. coelicolor* M1154/pAMX4. (B) Metabolic profile of pGP6783 expressed in GPAHex. HPLC traces are (i) WAC06783, (ii) *S. coelicolor* M1154/pAMX4, (iii) *S. coelicolor* M1154/pAMX4/pGP6783, (iv) *S. coelicolor* M1154/pAMX4/pGP6783/pIJ10257-staQ, and (v) the rimomycin-A standard. The HPLC trace was monitored at 280 nm. Trace amounts of rimomycin-A/B are also produced in WAC06783, as labeled with inverted triangles in the HPLC trace. (C) Chemical structures of rimomycin-A/B/C. The key COSY, HMBC, and NOSEY correlations indicating the three cross-links in rimomycin-A/B/C observed from the NMR spectra are labeled with bold lines, black curved arrows, and double-headed blue curved arrows, respectively.

tide antibiotics heterologous expression) synthetic biology platform.[16] Using GPAHex, two new cryptic GPAs, GP1416 and GP6738, were identified and characterized.

Here we describe the discovery and characterization of five novel type V GPAs—rimomycin-A/B/C (named for its BGC that is widely distributed in *Streptomyces rimosus* strains) and misaugamycin-A/B (named for its Mississauga, Ontario, Canada geographical source)—using phylogeny-guided genome mining of GPA BGCs coupled with heterologous expression using the GPAHex platform, which we improve through the addition of new regulatory elements. We show that these new GPAs are consistent with the type V subclass but have unprecedented structures, cross-linking patterns, and an improved antimicrobial spectrum. This study further demonstrates the power of GPAHex in mining novel cryptic GPAs.

RESULTS AND DISCUSSION

Phylogeny-Guided Genome Mining of Type V GPA BGCs. From published genomes and our in-house sequenced genomes, we identified 116 candidate BGCs using the GPA fingerprint sequences (*oxyB*, *oxyC*, *halI*, *dpgC*, and *oxyE*) and BLASTp followed by antiSMASH analysis.[30] All of the GPA BGCs were retrieved from organisms in the phylum Actinobacteria. Using the available whole genome sequences ($n = 97$), we constructed a multiple-species phylogeny tree using MinHash distances[31] (Figure 2A). Unlike our previous tree built using concatenated single-copy TIGRFam sequences,[32] MinHash distances use *k*mer information from the entire genome. Because most type V GPA BGCs are found in *Streptomyces* (kistamicin from *Nonomuraea* is the only exception), the associated strains are grouped in the top half of the tree and the D-Ala-D-Ala binding GPA BGCs are more widely distributed among other genera. Strains harboring more than one GPA BGC are indicated by multiple leaf nodes. Compared to the first description of the GPA BGCs species phylogeny tree, including 71 GPA BGCs,[29] we have dramatically expanded (18 vs 42) the number of identified type V GPA BGCs. These type V GPA BGCs represent an untapped reservoir of novel type V GPA chemical entities.

Strains containing the same GPA BGCs are closely related and form subclades (Figure 2A). For example, isolates possessing complestatin and GP6738 BGCs are clustered. Similarly, strains with corbomycin BGCs are grouped, but these are further split into two subclades, indicating that corbomycin BGC may have undergone mobilization events. Besides the complestatin, corbomycin, and GP6738 BGCs, two more GPA BGCs shared by different subclades attracted our attention. The rimomycin and misaugamycin BGCs (Figures 2B,C) are highly conserved in the clustered strains, and their domain structures are closely related to the complestatin BGCs. However, the structure and function of GPAs encoded by these two BGC subgroups are unknown, encouraging us to explore these candidates further. Beyond the known heptapeptide and nonapeptide scaffolds in the type V GPAs (Figures S1−S3), octapeptide and decapeptide scaffolds are also identified in our phylogenetic analysis (Figure 2A and Figures S4 and S5), indicating further chemical diversity in this subgroup of GPA.

GPAHex Production and Characterization of Rimomycin. The genome of WAC06783 was sequenced under our previous Illumina genome sequencing program

https://doi.org/10.1021/acscentsci.1c01389
ACS Cent. Sci. 2022, 8, 615−626

(ASM394757v1). Genome assembly resulted in 70 contigs, and the rimomycin BGC was identified in contig4 by antiSMASH[30] (Figure 2B and Table S3). The rimomycin BGC shares a significant similarity with the complestatin BGC (93% according to antiSMASH) except for the presence of a starter C domain and an E domain on its NPRS module 1, indicating a putative acyl tail modification on its N-terminal Hpg residue, which is in the D-configuration. A domain specificity prediction results in a heptapeptide scaffold sequence of Hpg-Trp-Hpg-Hpg-Hpg-(m)Tyr-Hpg, identical to that of complestatin.[18] The presence of the halogenase-encoding gene (*rmoL*) indicates that rimomycin should be chlorinated. The P450-$OxyA_{rmo}$ (RmoM) forms a monophyletic clade with the OxyA's from the corbomycin and GP6738 BGCs; however, the other P450-$OxyC_{rmo}$ (RmoN) forms a monophyletic clade distinct from the OxyC's from the complestatin, corbomycin, and GP6738 BGCs in the P450 phylogenetic tree (Figure S6). The P450s phylogeny indicates that there should be a canonical Trp2-Hpg4 biaryl cross-link in rimomycin. However, the other Hpg4-(m)Tyr6 biaryl ether cross-link may be shaped differently in rimomycin.

We could not detect significant GPA production by strain WAC06783 using our standard protocols.[15,33] Furthermore, WAC06783 was recalcitrant to genetic manipulation, complicated by its intrinsic resistance to kanamycin, apramycin, hygromycin, and others. We therefore turned to our GPAHex synthetic biology platform[16] to produce rimomycin and characterize its structure (Figure 3A). A 70,290 bp DNA fragment covering the predicted rimomycin BGC in the chromosome of WAC06783 was cloned into the pCGW vector using transformation-associated recombination (TAR) in yeast,[34] resulting in plasmid pGP6783 (Figure S7A,B). pGP6783 was mobilized into the GPAHex chassis strain, *Streptomyces coelicolor* M1154/pAMX4, through *Escherichia coli*−*Streptomyces* triparental mating[35] for heterologous expression. Comparative metabolic analysis of the high-performance liquid chromatography (HPLC) chromatograms identified a series of distinct peaks correlated to the introduction of pGP6783 (Figure 3B). High-resolution quadrupole time-of-flight mass spectrometry (HR-QTOF-MS) reveals three major signal mass values ($[M + H]^+$, m/z) of (A) 1121.3679, (B) 1155.3281, (C) 1189.2900 (Figure S8), correlating to the predicted molecular formulas $C_{61}H_{52}N_8O_{14}$ (A, calculated $[M + H]^+$: 1121.3681), $C_{61}H_{51}N_8O_{14}Cl$ (B, calculated $[M + H]^+$: 1155.3292), and $C_{61}H_{50}N_8O_{14}Cl_2$ (C, calculated $[M + H]^+$: 1189.2902). Compared to the molecular formula of complestatin, $C_{61}H_{45}N_7O_{15}Cl_6$, rimomycin has one additional nitrogen and hydrogen atom but lacks an oxygen atom. According to the nitrogen rule, the HRMS data indicates that rimomycin may have one free amine instead of the α-keto group in the starter unit of complestatin. Because rimomycin and complestatin possess 61 carbons, there should be no acylation on the N-terminal Hpg. Substituting a ketone group with an amine group results in a net increase of three hydrogen atoms. However, rimomycin possesses only one more hydrogen atom than complestatin, consistent with an additional intramolecular cross-link.

To elucidate the chemical structure of rimomycin, an overproduction strain was constructed by introducing the constitutively expressed *strR* regulator-*staQ*[19] driven by the ermEp* promoter in pIJ10257[36] into *S. coelicolor* M1154/pAMX4/pGP6783. The overexpression of *staQ* from A47934 BGC results in a 2-fold increase in A and a total 4.2-fold increase in all three rimomycin analogs (A, B, and C; Figure S9). Rimomycin-A was purified, and the structure was determined by one- and two-dimensional nuclear magnetic resonance spectrometry (1D/2D NMR) analyses (Figures S10−S16 and Table S5). The structure of rimomycin-A is shown in Figure 3C. As expected from the HRMS data, no acyl modification was observed, indicating that the C-starter domain may function as a structural domain to initiate the NRPS assembly line instead of catalyzing amide bond formation between an acyl group and the N-terminal free amine on Hpg1. The predicted extra A−*O*−B biaryl ether cross-link was assigned according to the observation of the key $^1H-^{13}C$ heteronuclear multiple bond correlations (HMBC) of H6 on ring A (A-H6 [δ 4.94 ppm]), C4 on ring B (B-C4 [δ 156.9 ppm]), and B-H5 (δ 7.25 ppm)/A-C5 (δ 150.5 ppm) (Figure S14). The A-*O*-B cross-link was further confirmed by the observation of the key nuclear Overhauser enhancement spectroscopy (NOSEY) correlations of A-H6 (δ 4.94 ppm)/B−H3 (δ 6.88 ppm), A-H6 (δ 4.94 ppm)/B-H5 (δ 7.25 ppm), and A-H6 (δ 4.94 ppm)/B−H6 (δ 8.00 ppm) (Figure S15). The C-*O*-D cross-link was assigned according to the observation of the $^1H-^{13}C$ HMBC correlations of C-H3 (δ 7.12 ppm)/D-C3 (δ 149.3 ppm) and C-H5 (δ 6.98 ppm)/D-C3 (δ 149.3 ppm), which was further confirmed by the observation of NOSEY correlations of C-H5 (δ 6.98 ppm)/D-H2 (δ 5.53 ppm) and C-H6 (δ 7.94 ppm)/D-H2 (δ 5.53 ppm) (Figure S15). The D-E cross-link was assigned according to the observation of the $^1H-^{13}C$ HMBC correlations of D-H6 (δ 5.18 ppm)/E-C6 (δ 134.8 ppm), E-H5 (δ 6.89 ppm)/D-C5 (δ 131.2 ppm), and E-H7 (δ 7.32 ppm)/D-C5 (δ 131.2 ppm) and was further confirmed by the observation of the NOSEY correlations of D-H6 (δ 5.18 ppm)/E-H4 (δ 7.50 ppm), D-H6 (δ 5.18 ppm)/E-H5 (δ 6.89 ppm), and D-H6 (δ 5.18 ppm)/E-H7 (δ 7.32 ppm) (Figure S15). Given that rimomycin-B and rimomycin-C are mono- and dichlorinated analogs of rimomycin-A, we first used tandem MS/MS to locate the chlorination sites on rimomycin-A. The MS_2 production ion fragments of rimomycin-A/B/C, as shown in Figure S17, clearly show the chlorination sites on rimomycin-B (Hpg5) and rimomycin-C (Hpg3 and Hpg5). The structures of rimomycin-B/-C were further confirmed through 1D/2D NMR spectrometry as shown in Figures S18−S29 and Tables S6 and S7. Along with kistamicin,[37] rimomycin is the second example of a type V GPA incorporating a 15-membered A-*O*-B ring linkage. Interestingly, we detected some production of rimomycin-A/B in the parental strain, WAC06783, after treating the crude extract with a 30% MeOH/H_2O (×3) wash, although we missed it in our initial analysis. A comparison of the crude extract of WAC06783 and the MeOH-treated samples showed that the rimomycin-A/B signal in the crude extract is masked by the massive production of oxytetracycline and rimocidin polyenes (Figure S30). Accordingly, we were able to locate the BGCs for oxytetracycline[38] and rimocidin[39] in the genome of WAC06783 (Figure S31). This masking of small quantities of a novel antibiotic by the production of known antimicrobial compounds further demonstrates the value of targeted discovery platforms such as GPAHex.

GPAHex Production and Characterization of Misaugamycin. The whole-genome sequence of WAC00631 was determined using a combination of Illumina and MinION nanopore platforms. Assembly using a hybrid approach generated a draft genome with 21 contigs, in which the misaugamycin BGC was identified on contig 4 using antiSMASH[30] (Figure 2C and Table S4). Like rimomycin, the misaugamycin BGC shows extensive similarity to the complestatin BGC (93% according to antiSMASH). The prediction of

https://doi.org/10.1021/acscentsci.1c01389
ACS Cent. Sci. 2022, 8, 615−626

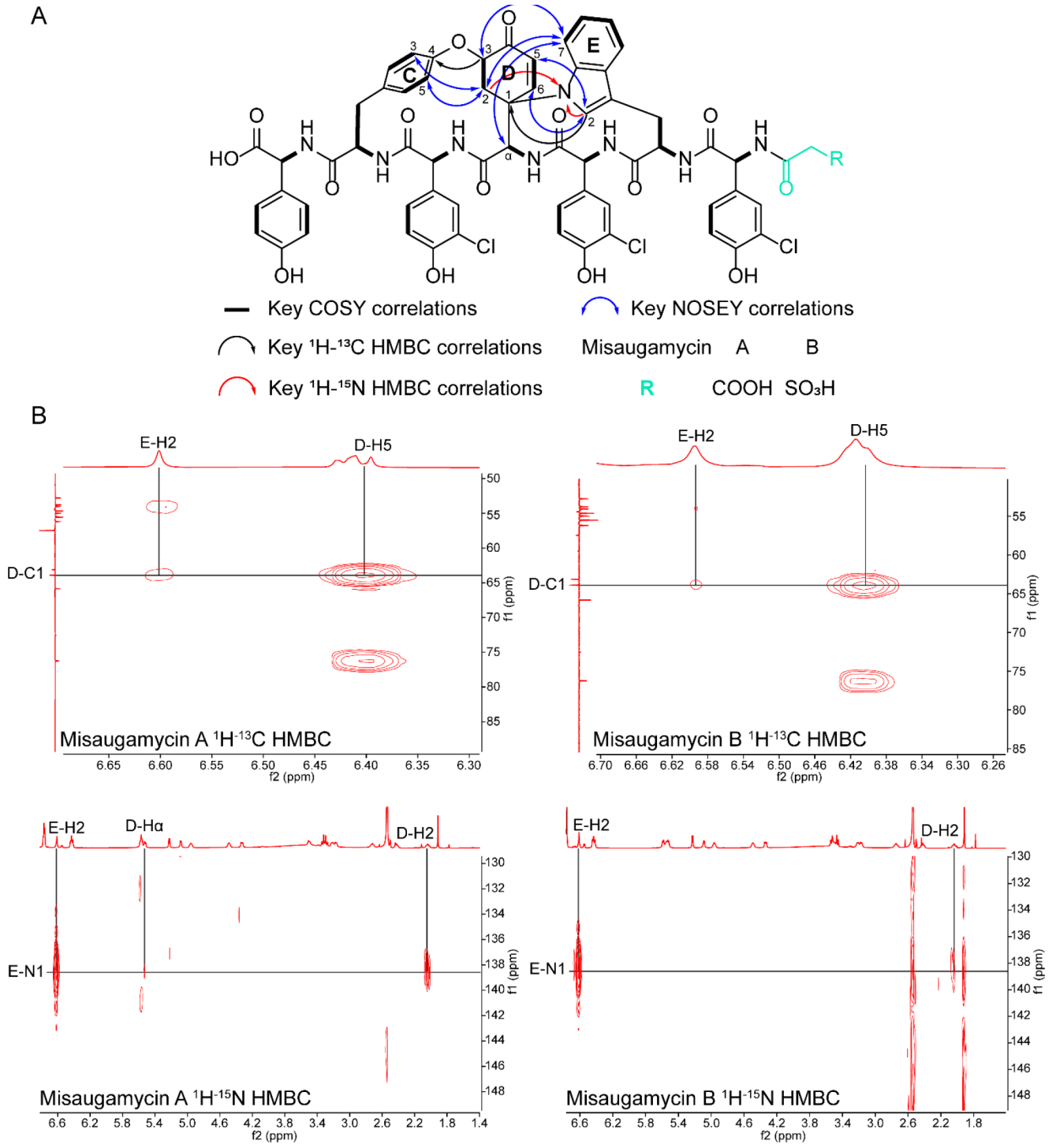

Figure 4. Discovery of misaugamycin from WAC00631 using GPAHex. (A) Chemical structures of misaugamycin-A/B. The central Hpg in misaugamycin-A/B has been reduced to form the unique ocHeg residue. The key COSY, HMBC, and NOSEY correlations observed from the NMR spectra are labeled with bold lines, black/red curved arrows, and blue double-headed curved arrows, respectively. The $^{1}H-^{15}N$ correlations (red arrows) observed in HMBC experiments are optimized for $^{n}J_{NH} = 8$ Hz.[40] Misaugamycin-A/B are differentiated by the substitution of the R group with carboxylic acid (A) or sulfonic acid (B) group. (B) 2D $^{1}H-^{13}C$ and $^{1}H-^{15}N$ HMBC spectra of the correlations between Trp2 and ocHeg4 residues in misaugamycin-A/B.

the A domain specificity reveals a heptapeptide scaffold of Hpg-Trp-Hpg-Hpg-Hpg-Tyr-Hpg, identical to that of rimomycin and complestatin. Because there is no MT domain in module 6, there should be a Tyr6 in misaugamycin instead of a mTyr6 in rimomycin and complestatin. A starter C domain was also identified in misaugamycin BGC, indicating the presence of a putative N-terminal acylated Hpg1. The presence of the halogenase encoding gene (*misH*) predicts that misaugamycin is chlorinated. P450-OxyC$_{mis}$ forms a monophyletic clade with the OxyCs from GP6738 and corbomycin BGCs; however, P450-OxyA$_{mis}$ forms a monophyletic clade distinct from the OxyAs in complestatin, corbomycin, GP6738, and rimomycin

https://doi.org/10.1021/acscentsci.1c01389
ACS Cent. Sci. 2022, 8, 615−626

Table 1. Minimum Inhibition Concentration (MIC) of GPAs

		MIC (μg/mL)								
					rimomycin			misaugamycin		
strains	resistance type	corbomycin	complestatin	kistamicin	A	B	C	A	B	vancomycin
E. coli BW25113		>128	>128	>128	>128	>128	>128	>128	>128	>128
E. coli BW25113Δ*bamB*Δ*tolC*		>128	>128	>128	8	8	4	>128	128	64
S. aureus ATCC 29213		2	2	2	4	2	2	8	4	1
S. aureus ATCC 33591		2	2	2	4	2	4	8	4	2
S. aureus USA300		8	8	4	16	4	4	8	4	1
S. aureus Mu3		4	4	2	8	2	4	16	4	2
S. aureus Mu50		2	2	1	4	1	2	8	4	4
B. subtilis 168		1	1	1	4	0.5	0.5	2	2	0.25
M. smegmatis ATCC 700084 (mc^{2}155)		>256	>256	>128	16	16	8	>256	>256	4
M. tuberculosis H37Ra		[a]	>128	[a]	4	[a]	[a]	[a]	[a]	2
E. faecalis ATCC 29212		8	8	4	8	2	4	16	16	4
E. faecium ATCC 19434		16	32	8	8	4	8	32	32	2
E. faecium ATCC 70022	VREA	16	32	8	8	2	4	64	32	>128
E. faecium WCC C0491		8	16	[a]	8	2	2	32	16	>128
E. faecium WCC C0492		8−16	16	[a]	16	4	8	32	16−32	>128
E. faecium WCC C0495		16	16	[a]	8	4	8	32	16	>128
E. faecium WCC C0500		4	8	[a]	4	4	4	16	16	>128
E. faecium WCC C0519		16	16	[a]	8	4	4	32	16	>128
E. faecium WCC C0533		16	16	[a]	16	4	4	64	32	>128
E. faecalis ATCC 51299	VREB	16	8	4	16	4	4	16	16	32
E. faecium WCC C0545		16	16	[a]	16	8	8	32	16	>128
E. faecium WCC C0558		8	16	[a]	16	4	8	32	16	>128

[a]Not determined.

BGCs in the P450 phylogenetic tree (Figure S6). On the basis of the P450 phylogeny, we predict a Hpg4-Tyr6 biaryl ether cross-link in misaugamycin. However, the characteristic Trp2-Hpg4 biaryl cross-link in the type V GPAs may be shaped differently in misaugamycin. Interestingly, a putative four-gene cassette *misNOPQ* encodes an acyl carrier protein (ACP), an acyl-CoA ligase, a phosphosulfolactate synthase, and a glyoxalase that appears to form one operon, surrounded by putative InsQ and IS200/IS605 transposase-encoding genes (*misL* and *misM*). The identical organization of the four genes cassette adjacent to the transposases was also identified in the genomes of *S. fradiae* ATCC 19609 and *S. fradiae* olg 1-1. However, in the genomes of *S. xinhaiensis* S187, *S. spectabilis* NRRL 2792, and *S.* sp. YIM121038, the two putative transposase genes are absent (Figure 2C). This cassette may have originated from *S. xinhaiensis* S187, *S. spectabilis* NRRL 2792, and *S.* sp. YIM121038 and was then mobilized into WAC00631, *S. fradiae* ATCC 19609, and *S. fradiae* olg 1-1 through horizontal gene transfer. We hypothesized that these genes are involved in the biosynthesis of the N-terminal acyl chain moiety of misaugamycin.

Because misaugamycin production was not detectable from the fermentation of WAC00631, we applied our GPAHex synthetic biology platform to its heterologous production. A 78,889 bp DNA region covering the predicted misaugamycin BGC in the chromosome of WAC00631 was cloned into pCGW using the identical TAR method in yeast,[34] resulting in pGP631 (Figure S7C,D). The pGP631 plasmid was mobilized into the GPAHex chassis strain, *S. coelicolor* M1154/pAMX4, for heterologous production. Comparative metabolomic analysis of the HPLC chromatograms revealed the production of a broad peak bearing the characteristic 280 nm UV absorption of GPAs (Figure S32). Misaugamycin is cryptic/silent in the parental strain, and expression in the GPAHex platform remained insufficient for downstream purification and structural elucidation; consequently, we turned to the introduction of StaQ as described above. As expected, the production of misaugamycin and analogs was dramatically improved in the *strR* overexpression strain (Figure S32).

The extract from *S. coelicolor* M1154/pAMX4/pGP631/pIJ10257-staQ was analyzed using HR-ESI-qTOF-MS, revealing two primary signal masses ($[M + H]^+$, m/z) of 1299.2675 and 1335.2338. These values respectively correspond to the predicted molecular formulas of $C_{63}H_{53}N_8O_{17}Cl_3$ (A, calculated $[M + H]^+$ = 1299.2673) and $C_{62}H_{53}N_8O_{18}SCl_3$ (B, calculated $[M + H]^+$ = 1335.2342) together with a series of related mass signals (Figure S33). Compared to complestatin, the molecular formula of misaugamycin indicates that there should be an introduction of a novel acyl/sulfur modification. Scaled-up (3 L) fermentation and purification through MeOH/H_2O extraction followed by LH20 and C18 reverse-phase semipreparative column chromatography results in two pure compounds, misaugamycin-A/B. An analysis of 1D and 2D NMR spectra (Figures S34−S50 and Tables S8 and S9) identified a novel type V GPA scaffold in which the central Hpg4 residue was reduced and tautomerized into a 4-oxocyclohex-2-en-1-ylglycine (ocHeg4) residue (Figure 4A). Moreover, the characteristic C6 (Trp2)-C5 (Hpg4) biaryl cross-link is replaced by an N1 (Trp2)-C1 (ocHeg4) cross-link. The previous C3 (Hpg4)-*O*-C4 (Tyr6) biaryl ether cross-link was transformed into a C3 (ocHeg4)-*O*-C4 (Tyr6) ether cross-link. The C-*O*-D cross-link was assigned according to the observation of the key $^1H-^{13}C$ HMBC correlation of D-H3 (δ 4.32 ppm)/C-C4 (δ 153.73 ppm), which was further confirmed by the observation of NOSEY correlations of D-H2 (δ 2.02 ppm)/C-H3 (δ 6.43 ppm) and D-H2 (δ 2.02 ppm)/C-H5 (δ 6.98 ppm) (Figures S39 and

https://doi.org/10.1021/acscentsci.1c01389
ACS Cent. Sci. 2022, 8, 615−626

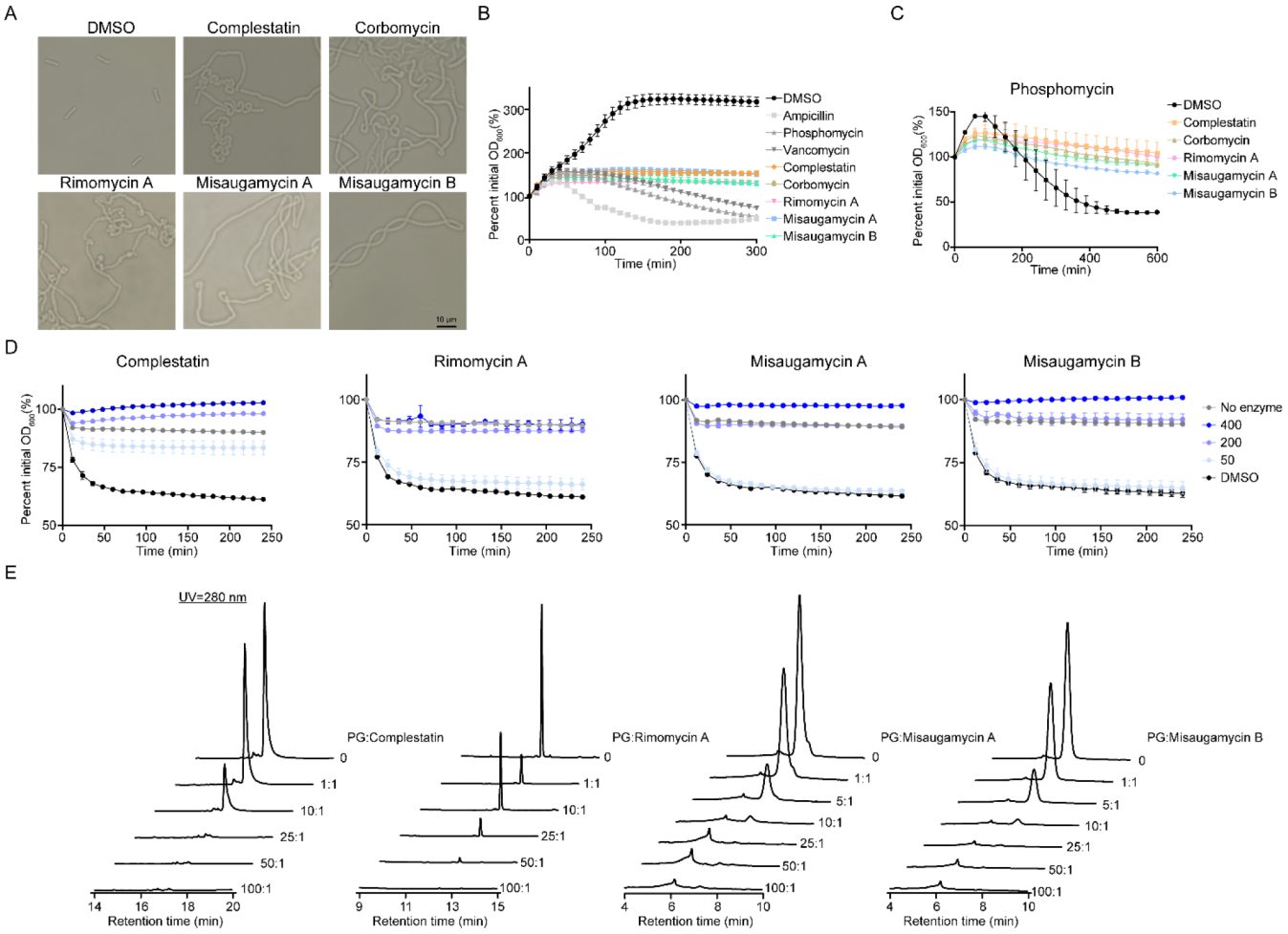

Figure 5. MOA studies of rimomycin and misaugamycin. (A) Bright-field microscopy of the morphology of *B. subtilis* 168 cells treated with type V GPAs. Like complestatin and corbomycin, rimomycin-A- and misaugamycin-A/B-treated cells show an extended and twisted phenotype. (B) Cell lytic assay of *B. subtilis* with various antibiotics. Rimomycin-A and misaugamycin-A/B, accompanied by complestatin and corbomycin, are bacteriostatic antibiotics. (C) Antagonization of cell lysis caused by the PG synthesis inhibitor, phosphomycin, by rimomycin-A and misaugamycin-A/B. (D) *In vitro* PG digestion by autolysin, LytD, in the presence of various concentrations (μg/mL) of complestatin, rimomycin-A, and misaugamycin-A/B. Means with error bars showing the standard deviation (s.d.) of triplicate experiments ($n = 3$) are plotted in panels B–D. (E) HPLC chromatograms of type V GPAs left unbound in solution after incubation with *B. subtilis* PG. GPAs and PG are mixed and incubated in various w/w ratios. The decreasing intensity of the corresponding GPA peak compared to the buffer control without PG represents compound binding and removal from solution. HPLC traces are monitored at 280 nm.

S47). The unprecedented N1 (Trp2)-C1 (ocHeg4) cross-link in misaugamycin-A/B was assigned by the observation of the key ^{1}H–^{13}C HMBC correlation of E-H2 (δ 6.60 ppm)/D-C1(δ 63.89 ppm) (Figure 4B and Figures S38 and S46) and the NOSEY correlations of D-H5 (δ 6.40 ppm)/E-H2 (δ 6.60 ppm), D-H6 (δ 7.94 ppm)/E-H2 (δ 6.60 ppm), D-H2 (δ 3.48, 2.02 ppm)/E-H7 (δ 8.13 ppm), D-H3 (δ 4.32 ppm)/E-H7 (δ 8.13 ppm), and D-Hα (δ 5.50 ppm)/E-H7(δ 8.13 ppm) (Figures S39 and S47). To confirm this unique N–C linkage, ^{1}H–^{15}N heteronuclear single quantum correlation (HSQC) experiments were performed. As expected, seven α-NH's from the heptapeptide scaffold were identified, and the indole amine signal was missing from the HSQC spectra for both misaugamycin-A/B (Figures S40 and S48). The N–C linkage was further supported by observing the key ^{1}H–^{15}N HMBC correlation of D-H2 (δ 2.02 ppm)/E-N1 (δ 138.5 ppm) for misaugamycin-A/B (Figure 4B and Figures S41 and S49). Additionally, the N-terminal Hpg was acylated by malonyl (misaugamycin-A) and 2-sulfoacetyl (misaugamycin-B) groups, which are both unprecedented GPA modifications. Using Na_2SO_3 to supplement the fermentation culture of *S. coelicolor* M1154/pAMX4/pGP631/pIJ-staQ led to the favored production of sulfonated misaugamycin-B (Figure S32).

Rimomycin and Misaugamycin-A/B Inhibit Autolysins. Type V GPAs show potent antibacterial activity against multiple Gram-positive bacteria, including multi-drug-resistant pathogens.[15,16] These GPAs display a novel MOA by blocking autolysin action through binding to PG, distinct from conventional GPAs that bind to the terminal D-Ala-D-Ala on the PG stem peptide.[15] Rimomycin-A/B/C and misaugamycin-A/B show broad-spectrum antibacterial activity against Gram-positive bacteria, including methicillin-resistant *S. aureus* (MRSA) and vancomycin-resistant enterococci (VREA and VREB) (Table 1). Interestingly, rimomycin-A/B/C show a broader antibacterial spectrum with additional antibacterial activity against the efflux pump and outer-membrane-compromised *E. coli* BW25113 Δ*bamB*Δ*tolC*, *Mycobacterium smegmatis* mc^{2}155, and *Mycobacterium tuberculosis* H37Ra, which has not been observed in other type V GPAs. Kistamicin possesses an A-*O*-B/C-*O*-D/D-E tricyclic scaffold identical to that of

https://doi.org/10.1021/acscentsci.1c01389
ACS Cent. Sci. 2022, 8, 615–626

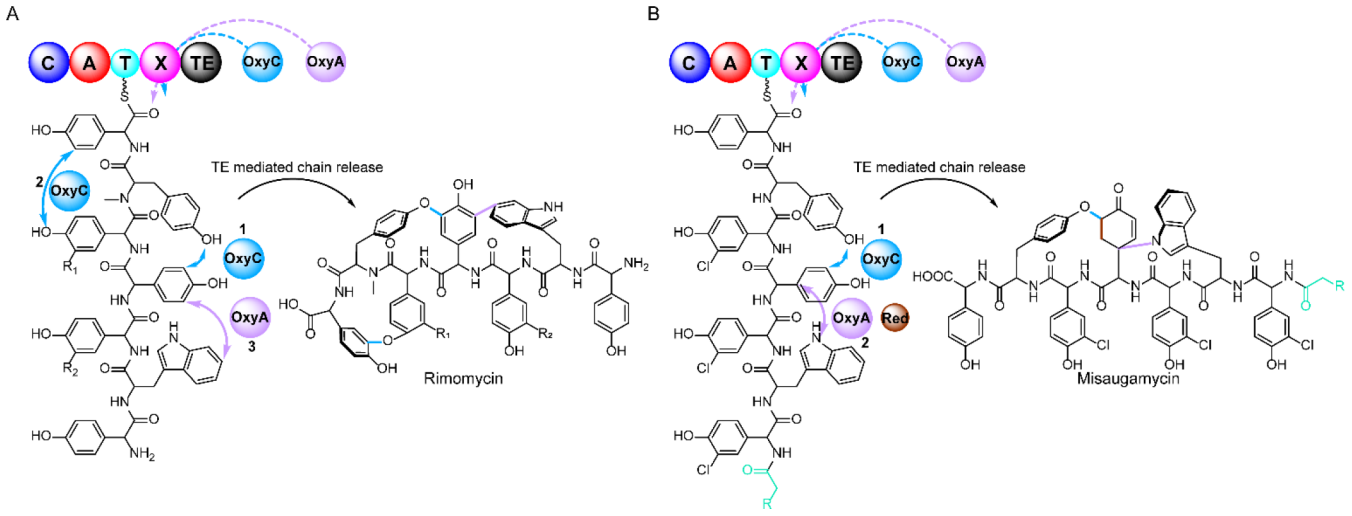

Figure 6. Proposed biosyntheses of (A) rimomycin and (B) misaugamycin. OxyA and OxyC in rimomycin and misaugamycin BGCs are recruited to the NRPS-tethered heptapeptide substrates by the conserved X-domain to mediate the oxidative cyclization. Because $OxyC_{rmo}$ is located in a distinct clade from $OxyC_{kis}$ in the P450 phylogenetic tree, we proposed the following ring-closure sequence in rimomycin biosynthesis: C-*O*-D (1) > A-*O*-B (2) > D-E (3). A typical C-*O*-D (1) > D-E (2) ring-closure sequence was proposed for misaugamycin biosynthesis. During the closure of the D-E ring through the unprecedented C−N linkage catalyzed by $OxyA_{mis}$ in misaugamycin biosynthesis, the F_{420}-dependent reductase, MisW, is proposed to take part in the reduction of the central Hpg4 to form ocHeg4. Ring-closed heptapeptide scaffolds are cleaved from the NRPS assembly line by the terminal TE domain to release rimomycin and misaugamycin.

rimomycin; therefore, we purified this compound from the producer *Nonomuraea* sp. ATCC 55076. Kistamicin shows no activity against *E. coli* BW25113 Δ*bamB*Δ*tolC* and *M. smegmatis* mc^2155 (Table 1). The subtle changes in the peptide scaffold by introducing *N*-methylation on Tyr6 and substituting Tyr1 and Dpg3 with Hpg may empower rimomycin with broader activity compared to that of kistamicin. As observed in the type I−IV GPAs, halogenation generally improves the antibacterial activity of rimomycin-B/C. Although misaugamycin-A shows slightly weaker antibacterial activity than the other type V GPAs, its N-terminal 2-sulfoacetyl congener, misaugamycin-B, shows improved activity compared to that of other type V GPAs.

To better understand the MOA of rimomycin and misaugamycin, phenotypic and *in vitro* PG digestion and binding assays were performed. Like the known type V GPAs complestatin and corbomycin, rimomycin A and misaugamycin-A/B induce a twisted and extended growth morphology to *Bacillus subtilis* 168 (Figure 5A) and are bacteriostatic (Figure 5B). Furthermore, rimomycin A and misaugamycin-A/B block cell lysis induced by PG synthesis inhibitors, ampicillin, and phosphomycin (Figure 5C and Figure S51) and inhibit *in vitro* cell wall degradation by the PG hydrolases, LytD and CwlO (Figure 5D and Figure S52). *In vitro* PG binding assays demonstrate that PG binds rimomycin-A and misaugamycin-A/B and can remove the compounds from solution (Figure 5E and Figure S53). Interestingly, rimomycin-A was titrated from solution by PG more efficiently at 1:1 w/w PG/rimomycin-A than at 10:1 w/w PG/rimomycin-A when using *B. subtilis* PG, which has never been observed in other type V GPAs. This may indicate that rimomycin-A has additional binding sites on *B. subtilis* PG, explaining its broader antibacterial spectrum. Overall, rimomycin-A and misaugamycin-A/B have MOAs similar to those of complestatin and corbomycin by binding to the PG, preventing the action of autolysins. Further in-depth studies are required to characterize the binding sites of rimomycin and misaugamycin on PG to understand their MOAs fully.

CONCLUSIONS

GPAs are essential for treating infections caused by multi-drug-resistant Gram-positive pathogens. However, the emergence of GPA resistance threatens the efficacy of these antibiotics, so more effective GPAs are needed to help address the antibiotic resistance crisis.[12] Although medicinal chemists have begun to address this problem by introducing second-generation GPAs, such as telavancin, dalbavancin, and oritavancin, into the clinic to combat VRE, there remains a need for novel GPAs with distinct MOAs to offer alternative strategies for the treatment of infections caused by multi-drug-resistant Gram-positive pathogens. Recently, our group characterized members of the poorly studied type V GPA subclass including complestatin, corbomycin, and GP6738 that inhibit bacterial cell division by binding to the PG and consequently blocking the activity of autolysins.[15,16] This MOA is distinct from the D-Ala-D-Ala binding of other GPAs, enabling the type V GPAs to evade canonical GPA resistance. Expanding the type V GPA chemical diversity offers a promising direction for drug discovery and development.

The advances in genome sequencing have uncovered countless BGCs in the bacterial pan-genome, especially in Actinobacteria, that may encode novel antibiotics.[41] Using a phylogeny-guided genome mining approach,[29] we identified 116 GPA BGCs from public genomes and our in-house sequenced genomes. Many of these GPA clusters belong to the type V GPAs, primarily identified in the genomes of *Streptomyces*, and represent an extensive reservoir of type V GPA chemical dark matter. Among them, rimomycin and misaugamycin were shared by several *Streptomyces* strains. Combined with the GPAHex synthetic biology platform,[16] we captured the two BGCs for heterologous expression. Rimomycin production was increased by 8.5-fold in GPAHex and 37.5-fold when coupled with the overexpression of the StrR regulator compared to the parental strain. Similarly, we were able to express the cryptic/silent misaugamycin BGC in GPAHex and boost the production of misaugamycin-A/B when coupled with the overexpression of

https://doi.org/10.1021/acscentsci.1c01389
ACS Cent. Sci. 2022, 8, 615−626

the StrR regulator. As a master regulator of GPA biosynthesis, *strR* overexpression can significantly increase the output of GPAs.[42−44] In our case, *staQ*, the *strR* from the A47934 BGC, was overexpressed instead of the BGC-associated *strR*, indicating that *staQ* can be applied as a general tool to promote GPA production.

Rimomycin-A/B/C and misaugamycin-A/B, new members of the type V GPA subclass, exhibit striking structural novelty. Compared to the typical C-*O*-D and D-E bicrosslinked scaffold of the type V GPA,[13] rimomycin-A/B/C possess an additional 15-membered A-*O*-B ring, a feature that is also observed in kistamicin.[20] However, there are only two P450s present in both BGCs despite the presence of three cross-links. Given the difference between the biaryl ether and biaryl linkages, the OxyC protein is believed to catalyze the two biaryl ether cross-links, and the OxyA protein is thought to build the biaryl cross-link. *In vivo* gene inactivation and *in vitro* reconstitution studies in kistamicin biosynthesis support this hypothesis.[20] It is proposed that the maturation of kistamicin biosynthesis undergoes a sequential cross-linking of C-*O*-D > D-E > A-*O*-B ring.[20] However, $OxyC_{kis}$ clusters more closely to the OxyC proteins from the D-Ala-D-Ala binding GPA BGCs instead of the OxyC proteins from the type V GPA BGCs in the P450 phylogenetic tree (Figure S6). Within the typical OxyC proteins from the type V GPA BGCs, $OxyC_{rmo}$ proteins form a monophyletic clade separate from ComJ and the OxyC proteins from the BGCs of corbomycin, GP6738, and misaugamycin. This may indicate that cross-linking in rimomycin biosynthesis is distinct from that of kistamicin (Figure 6A). Further studies are ongoing to elucidate the mechanism for the P450-catalyzed cross-linking in rimomycin-A/B/C biosynthesis.

Misaugamycin-A/B are distinct from all previously described GPAs, recruiting malonyl and 2-sulfoacetyl groups as the acyl tails and installing a reduced and tautomerized central Hpg4 and a unique C−N linkage between ocHeg4 and Trp2. The four-gene cassette, including an ACP, an acyl-CoA ligase, a phosphosulfolactate synthetase, and a glyoxalase encoding gene, is predicted to be responsible for the supply of the 2-sulfoacetyl group (Figure S54). We propose that the terminal F_{420}-dependent oxidoreductase coding gene that is conserved across the misaugamycin-like BGCs accounts for the reduction of Hpg4. The unique C−N linkage is predicted to be installed by the $OxyA_{mis}$ protein, which catalyzes the C−C biaryl linkage between Hpg4 and Trp2 in all of the other type V GPAs (Figure 6B). Although rimomycin-A/B/C and misaugamycin-A/B show distinct cross-link patterns, the X-domain-mediated recruitment of Oxys to perform the oxidative cyclization seems to be conserved in their biosynthesis as observed in other GPAs. The sequence alignment of $OxyA_{rmo}$/$OxyC_{rmo}$ and $OxyA_{mis}$/$OxyC_{mis}$ reveals the presence of the conserved characteristic X-domain recruitment fingerprint "PRDD" motif in the F-helix and the presence of characteristic X-domain interaction residues in the D-, E-, F-, and G-helixes[28] (Figure S55). These features suggest that the $OxyC_{rmo}$-catalyzed multiplex biaryl-ether cross-link and the $OxyA_{mis}$-catalyzed C−N cross-link should all be mediated by the interaction between the Oxy proteins and the penultimate X-domain on the NRPS.[28] Additional in-depth *in vivo* and *in vitro* studies are required to clarify the details of the biosynthetic mechanisms of these novel compounds.

Rimomycin-A/B/C and misaugamycin-A/B, like the previously characterized complestatin, corbomycin, and GP6738, interrupt the cell wall degradation steps essential for cell division by blocking the activity of autolysins.[15,16] The conserved C-*O*-D and D-E dual-ring structure present in type V GPAs is the essential structural motif to exhibit their antibacterial activity. Reconstruction of the C-*O*-D and D-E dual-ring linkage through reduction of the central Hpg4 to ocHpg4 and the installation of the C−N-linked D-E ring in misaugamycin preserves its autolysins' inhibition MOA. However, the more compressed 12-membered D-E ring in misaugamycin compared to the more common 16-membered D-E ring in complestatin, corbomycin, kistamicin, and rimomycin impaired its antibacterial activity. Alternatively, the unprecedent N-terminal acylation (2-sulfoacetyl) modification was introduced to compensate for the potency of misaugamycin. The more rigid 3D structures constructed by the installation of additional cross-links in the peptide scaffold of the type V GPAs (A-*O*-B cross-link in rimomycin/kistamicin and B-C/G-*O*-H cross-links in corbomycin) may increase the affinity of the GPAs for PG, contributing to improved antibacterial efficacy.[16] Beyond the variations in the ring topology, chlorination modification can also improve the antibacterial activity in the type V GPAs. Interestingly, rimomycin-A/B/C show additional antimycobacterial activity and antibacterial activity against the efflux pump and the outer-membrane-compromised *E. coli* BW25113 Δ*bamB*Δ*tolC* strain and improved efficacy against VRE compared to other type V GPAs. We note that rimomycin-A/B/C possess a free N-terminal amino group, providing a suitable site for semisynthesis differentiation to generate new derivatives with improved druglike properties.

The type V GPAs show a novel MOA with low resistance development, properties coveted in drug discovery to mitigate the antibiotic resistance crisis. Expanding this novel functional class of GPAs offers a promising avenue for the development of new drug leads. Phylogenetic analysis revealed dozens of novel GPA BGCs in bacterial genomes, especially those of *Streptomyces*. As the growth of sequenced bacterial genomes continues, many more hidden natural product BGCs encoding unknown molecules will be brought to light. The combination of genomics and synthetic biology has the potential to accelerate innovations in the drug discovery pipeline.

■ ASSOCIATED CONTENT

Supporting Information

The Supporting Information is available free of charge at https://pubs.acs.org/doi/10.1021/acscentsci.1c01389.

Materials and methods, mass spectra, and 1D/2D NMR spectra of all compounds (DOCX)

All information on the strains possessing GPA BGC identified in this study (XLSX)

■ AUTHOR INFORMATION

Corresponding Author

Gerard D. Wright − *David Braley Center for Antibiotic Discovery, Michael G. DeGroote Institute for Infectious Disease Research, Department of Biochemistry and Biomedical Sciences, McMaster University, Hamilton, Ontario L8N 3Z5, Canada;* orcid.org/0000-0002-9129-7131; Email: wrightge@mcmaster.ca

Authors

Min Xu − *David Braley Center for Antibiotic Discovery, Michael G. DeGroote Institute for Infectious Disease Research, Department of Biochemistry and Biomedical Sciences,*

https://doi.org/10.1021/acscentsci.1c01389
ACS Cent. Sci. 2022, 8, 615−626

McMaster University, Hamilton, Ontario L8N 3Z5, Canada; orcid.org/0000-0002-6661-5177

Wenliang Wang − *David Braley Center for Antibiotic Discovery, Michael G. DeGroote Institute for Infectious Disease Research, Department of Biochemistry and Biomedical Sciences, McMaster University, Hamilton, Ontario L8N 3Z5, Canada*

Nicholas Waglechner − *David Braley Center for Antibiotic Discovery, Michael G. DeGroote Institute for Infectious Disease Research, Department of Biochemistry and Biomedical Sciences, McMaster University, Hamilton, Ontario L8N 3Z5, Canada*

Elizabeth J. Culp − *David Braley Center for Antibiotic Discovery, Michael G. DeGroote Institute for Infectious Disease Research, Department of Biochemistry and Biomedical Sciences, McMaster University, Hamilton, Ontario L8N 3Z5, Canada*

Allison K. Guitor − *David Braley Center for Antibiotic Discovery, Michael G. DeGroote Institute for Infectious Disease Research, Department of Biochemistry and Biomedical Sciences, McMaster University, Hamilton, Ontario L8N 3Z5, Canada*

Complete contact information is available at: https://pubs.acs.org/10.1021/acscentsci.1c01389

Author Contributions

M.X. and G.D.W. conceived the study and designed the experiments. W.W. performed the purification and structural elucidation of the compounds. N.W. performed the genome assembly of the Illumina genome sequencing data and the bioinformatics analysis of the glycopeptide antibiotics biosynthetic gene clusters. E.J.C. purified the peptidoglycan and autolysins. A.K.G. performed the nanopore genome sequencing and genome assembly of WAC00631. M.X. performed all of the other experiments. M.X. and G.D.W. wrote the paper with input from all authors.

Notes

The authors declare no competing financial interest.

■ ACKNOWLEDGMENTS

We thank Dr. Bob Berno and Dr. Hilary A. Jenkins for help with the nitrogen NMR and Dr. Kalinka Koteva for help with the tandem MS/MS. We thank Dr. Michael Cook for testing the MIC against *M. tuberculosis* H37Ra. We also thank Haley Zubyk for suggesting the name misaugamycin. This research was funded by the Canadian Institutes of Health Research (grant FRN-148463), the Natural Sciences and Engineering Research Council (grant 237480), the Ontario Research Fund, and a Canada Research Chair to G.D.W. E.J.C. was supported by a CIHR Vanier Canada Graduate Scholarship. N.W. and A.K.G. were supported by a CIHR Canada Graduate Scholarship Doctoral Award.

■ REFERENCES

(1) Zeng, D.; Debabov, D.; Hartsell, T. L.; Cano, R. J.; Adams, S.; Schuyler, J. A.; McMillan, R.; Pace, J. L. Approved Glycopeptide Antibacterial Drugs: Mechanism of Action and Resistance. *Cold Spring Harb Perspect. Med.* **2016**, *6* (12), a026989.

(2) Pootoolal, J.; Neu, J.; Wright, G. D. Glycopeptide antibiotic resistance. *Annu. Rev. Pharmacol. Toxicol.* **2002**, *42*, 381−408.

(3) Sheldrick, G. M.; Jones, P. G.; Kennard, O.; Williams, D. H.; Smith, G. A. Structure of vancomycin and its complex with acetyl-D-alanyl-D-alanine. *Nature* **1978**, *271* (5642), 223−5.

(4) Bugg, T. D.; Dutka-Malen, S.; Arthur, M.; Courvalin, P.; Walsh, C. T. Identification of vancomycin resistance protein VanA as a D-alanine:D-alanine ligase of altered substrate specificity. *Biochemistry* **1991**, *30* (8), 2017−21.

(5) Bugg, T. D.; Wright, G. D.; Dutka-Malen, S.; Arthur, M.; Courvalin, P.; Walsh, C. T. Molecular basis for vancomycin resistance in *Enterococcus faecium* BM4147: biosynthesis of a depsipeptide peptidoglycan precursor by vancomycin resistance proteins VanH and VanA. *Biochemistry* **1991**, *30* (43), 10408−15.

(6) Wu, Z.; Wright, G. D.; Walsh, C. T. Overexpression, purification, and characterization of VanX, a D-, D-dipeptidase which is essential for vancomycin resistance in *Enterococcus faecium* BM4147. *Biochemistry* **1995**, *34* (8), 2455−63.

(7) Cui, L.; Ma, X.; Sato, K.; Okuma, K.; Tenover, F. C.; Mamizuka, E. M.; Gemmell, C. G.; Kim, M. N.; Ploy, M. C.; El-Solh, N.; et al. Cell wall thickening is a common feature of vancomycin resistance in *Staphylococcus aureus*. *J. Clin. Microbiol.* **2003**, *41* (1), 5−14.

(8) Cui, L.; Iwamoto, A.; Lian, J. Q.; Neoh, H. M.; Maruyama, T.; Horikawa, Y.; Hiramatsu, K. Novel mechanism of antibiotic resistance originating in vancomycin-intermediate *Staphylococcus aureus*. *Antimicrob. Agents Chemother.* **2006**, *50* (2), 428−38.

(9) Malabarba, A.; Ciabatti, R.; Scotti, R.; Goldstein, B. P.; Ferrari, P.; Kurz, M.; Andreini, B. P.; Denaro, M. New semisynthetic glycopeptides MDL 63,246 and MDL 63,042, and other amide derivatives of antibiotic A-40,926 active against highly glycopeptide-resistant VanA enterococci. *J. Antibiot. (Tokyo)* **1995**, *48* (8), 869−83.

(10) Cooper, R. D.; Snyder, N. J.; Zweifel, M. J.; Staszak, M. A.; Wilkie, S. C.; Nicas, T. I.; Mullen, D. L.; Butler, T. F.; Rodriguez, M. J.; Huff, B. E.; et al. Reductive alkylation of glycopeptide antibiotics: synthesis and antibacterial activity. *J. Antibiot. (Tokyo)* **1996**, *49* (6), 575−81.

(11) Leadbetter, M. R.; Adams, S. M.; Bazzini, B.; Fatheree, P. R.; Karr, D. E.; Krause, K. M.; Lam, B. M.; Linsell, M. S.; Nodwell, M. B.; Pace, J. L.; et al. Hydrophobic vancomycin derivatives with improved ADME properties: discovery of telavancin (TD-6424). *J. Antibiot. (Tokyo)* **2004**, *57* (5), 326−36.

(12) Blaskovich, M. A. T.; Hansford, K. A.; Butler, M. S.; Jia, Z.; Mark, A. E.; Cooper, M. A. Developments in Glycopeptide Antibiotics. *ACS Infect. Dis.* **2018**, *4* (5), 715−735.

(13) Nicolaou, K. C.; Boddy, C. N.; Brase, S.; Winssinger, N. Chemistry, Biology, and Medicine of the Glycopeptide Antibiotics. *Angew. Chem., Int. Ed.* **1999**, *38* (15), 2096−2152.

(14) Yim, G.; Thaker, M. N.; Koteva, K.; Wright, G. Glycopeptide antibiotic biosynthesis. *J. Antibiot. (Tokyo)* **2014**, *67* (1), 31−41.

(15) Culp, E. J.; Waglechner, N.; Wang, W.; Fiebig-Comyn, A. A.; Hsu, Y. P.; Koteva, K.; Sychantha, D.; Coombes, B. K.; Van Nieuwenhze, M. S.; Brun, Y. V.; et al. Evolution-guided discovery of antibiotics that inhibit peptidoglycan remodelling. *Nature* **2020**, *578* (7796), 582−587.

(16) Xu, M.; Wang, W.; Waglechner, N.; Culp, E. J.; Guitor, A. K.; Wright, G. D. GPAHex-A synthetic biology platform for Type IV-V glycopeptide antibiotic production and discovery. *Nat. Commun.* **2020**, *11* (1), 5232.

(17) van Wageningen, A. M.; Kirkpatrick, P. N.; Williams, D. H.; Harris, B. R.; Kershaw, J. K.; Lennard, N. J.; Jones, M.; Jones, S. J.; Solenberg, P. J. Sequencing and analysis of genes involved in the biosynthesis of a vancomycin group antibiotic. *Chem. & Biol.* **1998**, *5* (3), 155−62.

(18) Chiu, H. T.; Hubbard, B. K.; Shah, A. N.; Eide, J.; Fredenburg, R. A.; Walsh, C. T.; Khosla, C. Molecular cloning and sequence analysis of the complestatin biosynthetic gene cluster. *Proc. Natl. Acad. Sci. U. S. A.* **2001**, *98* (15), 8548−53.

(19) Pootoolal, J.; Thomas, M. G.; Marshall, C. G.; Neu, J. M.; Hubbard, B. K.; Walsh, C. T.; Wright, G. D. Assembling the glycopeptide antibiotic scaffold: The biosynthesis of A47934 from *Streptomyces toyocaensis* NRRL15009. *Proc. Natl. Acad. Sci. U. S. A.* **2002**, *99* (13), 8962−7.

(20) Greule, A.; Izore, T.; Iftime, D.; Tailhades, J.; Schoppet, M.; Zhao, Y.; Peschke, M.; Ahmed, I.; Kulik, A.; Adamek, M.; et al.

Kistamicin biosynthesis reveals the biosynthetic requirements for production of highly crosslinked glycopeptide antibiotics. *Nat. Commun.* **2019**, *10* (1), 2613.
(21) Kittila, T.; Kittel, C.; Tailhades, J.; Butz, D.; Schoppet, M.; Buttner, A.; Goode, R. J. A.; Schittenhelm, R. B.; van Pee, K. H.; Sussmuth, R. D.; et al. Halogenation of glycopeptide antibiotics occurs at the amino acid level during non-ribosomal peptide synthesis. *Chem. Sci.* **2017**, *8* (9), 5992−6004.
(22) Leng, D. J.; Greule, A.; Cryle, M. J.; Tosin, M. Chemical probes reveal the timing of early chlorination in vancomycin biosynthesis. *Chem. Commun.* **2021**, *57* (18), 2293−2296.
(23) Stinchi, S.; Carrano, L.; Lazzarini, A.; Feroggio, M.; Grigoletto, A.; Sosio, M.; Donadio, S. A derivative of the glycopeptide A40926 produced by inactivation of the beta-hydroxylase gene in Nonomuraea sp. ATCC39727. *FEMS Microb. Lett.* **2006**, *256* (2), 229−35.
(24) Forneris, C. C.; Seyedsayamdost, M. R. In Vitro Reconstitution of OxyC Activity Enables Total Chemoenzymatic Syntheses of Vancomycin Aglycone Variants. *Angew. Chem., Int. Ed.* **2018**, *57* (27), 8048−8052.
(25) Tailhades, J.; Zhao, Y.; Ho, Y. T. C.; Greule, A.; Ahmed, I.; Schoppet, M.; Kulkarni, K.; Goode, R. J. A.; Schittenhelm, R. B.; De Voss, J. J.; et al. A Chemoenzymatic Approach to the Synthesis of Glycopeptide Antibiotic Analogues. *Angew. Chem., Int. Ed.* **2020**, *59* (27), 10899−10903.
(26) Zhao, Y.; Goode, R. J. A.; Schittenhelm, R. B.; Tailhades, J.; Cryle, M. J. Exploring the Tetracyclization of Teicoplanin Precursor Peptides through Chemoenzymatic Synthesis. *J. Org. Chem.* **2020**, *85* (3), 1537−1547.
(27) Peschke, M.; Gonsior, M.; Sussmuth, R. D.; Cryle, M. J. Understanding the crucial interactions between Cytochrome P450s and non-ribosomal peptide synthetases during glycopeptide antibiotic biosynthesis. *Curr. Opin. Struct. Biol.* **2016**, *41*, 46−53.
(28) Haslinger, K.; Peschke, M.; Brieke, C.; Maximowitsch, E.; Cryle, M. J. X-domain of peptide synthetases recruits oxygenases crucial for glycopeptide biosynthesis. *Nature* **2015**, *521* (7550), 105−9.
(29) Waglechner, N.; McArthur, A. G.; Wright, G. D. Phylogenetic reconciliation reveals the natural history of glycopeptide antibiotic biosynthesis and resistance. *Nat. Microbiol.* **2019**, *4* (11), 1862−1871.
(30) Blin, K.; Shaw, S.; Steinke, K.; Villebro, R.; Ziemert, N.; Lee, S. Y.; Medema, M. H.; Weber, T. antiSMASH 5.0: updates to the secondary metabolite genome mining pipeline. *Nucleic Acids Res.* **2019**, *47* (W1), W81−W87.
(31) Katz, L. S.; Griswold, T.; Morrison, S. S.; Caravas, J. A.; Zhang, S.; den Bakker, H. C.; Deng, X.; Carleton, H. A. Mashtree: a rapid comparison of whole genome sequence files. *J.Open Source Softw.* **2019**, *4* (44), 1762.
(32) Selengut, J. D.; Haft, D. H.; Davidsen, T.; Ganapathy, A.; Gwinn-Giglio, M.; Nelson, W. C.; Richter, A. R.; White, O. TIGRFAMs and Genome Properties: tools for the assignment of molecular function and biological process in prokaryotic genomes. *Nucleic Acids Res.* **2007**, *35* (Database issue), D260−D264.
(33) Thaker, M. N.; Wang, W.; Spanogiannopoulos, P.; Waglechner, N.; King, A. M.; Medina, R.; Wright, G. D. Identifying producers of antibacterial compounds by screening for antibiotic resistance. *Nat. Biotechnol.* **2013**, *31* (10), 922−7.
(34) Zhang, J. J.; Yamanaka, K.; Tang, X.; Moore, B. S. Direct cloning and heterologous expression of natural product biosynthetic gene clusters by transformation-associated recombination. *Methods Enzymol.* **2019**, *621*, 87−110.
(35) Kieser, T., et al. *Practical Streptomyces Genetics*, 2nd ed.; John Innes Foundation: Norwich, U.K., 2000.
(36) Hong, H. J.; Hutchings, M. I.; Hill, L. M.; Buttner, M. J. The role of the novel Fem protein VanK in vancomycin resistance in *Streptomyces coelicolor*. *J. Biol. Chem.* **2005**, *280* (13), 13055−61.
(37) Naruse, N.; Tenmyo, O.; Kobaru, S.; Hatori, M.; Tomita, K.; Hamagishi, Y.; Oki, T. New antiviral antibiotics, kistamicins A and B. I. Taxonomy, production, isolation, physico-chemical properties and biological activities. *J. Antibiot. (Tokyo)* **1993**, *46* (12), 1804−11.
(38) Zhang, W.; Ames, B. D.; Tsai, S. C.; Tang, Y. Engineered biosynthesis of a novel amidated polyketide, using the malonamyl-specific initiation module from the oxytetracycline polyketide synthase. *Appl. Environ. Microbiol.* **2006**, *72* (4), 2573−80.
(39) Seco, E. M.; Perez-Zuniga, F. J.; Rolon, M. S.; Malpartida, F. Starter unit choice determines the production of two tetraene macrolides, rimocidin and CE-108, in *Streptomyces diastaticus* var. 108. *Chem. & Biol.* **2004**, *11* (3), 357−66.
(40) Wang, D.; Jiang, W.; Kim, C. K.; Bokesch, H. R.; Woldemichael, G. M.; Gryder, B. E.; Shern, J. F.; Khan, J.; O'Keefe, B. R.; Beutler, J. A.; et al. Neopetrothiazide: An Intriguing Pentacyclic Thiazide Alkaloid from the Sponge *Neopetrosia* sp. *Org. Lett.* **2021**, *23* (9), 3278−3281.
(41) Kautsar, S. A.; Blin, K.; Shaw, S.; Weber, T.; Medema, M. H. BiG-FAM: the biosynthetic gene cluster families database. *Nucleic Acids Res.* **2021**, *49* (D1), D490−D497.
(42) Horbal, L.; Kobylyanskyy, A.; Yushchuk, O.; Zaburannyi, N.; Luzhetskyy, A.; Ostash, B.; Marinelli, F.; Fedorenko, V. Evaluation of heterologous promoters for genetic analysis of *Actinoplanes teichomyceticus*–Producer of teicoplanin, drug of last defense. *J. Biotechnol.* **2013**, *168* (4), 367−72.
(43) Lo Grasso, L.; Maffioli, S.; Sosio, M.; Bibb, M.; Puglia, A. M.; Alduina, R. Two Master Switch Regulators Trigger A40926 Biosynthesis in *Nonomuraea* sp. Strain ATCC 39727. *J. Bacteriol.* **2015**, *197* (15), 2536−44.
(44) Li, X.; Zhang, C.; Zhao, Y.; Lei, X.; Jiang, Z.; Zhang, X.; Zheng, Z.; Si, S.; Wang, L.; Hong, B. Comparative genomics and transcriptomics analyses provide insights into the high yield and regulatory mechanism of Norvancomycin biosynthesis in *Amycolatopsis orientalis* NCPC 2−48. *Microb. Cell Fact.* **2021**, *20* (1), 28.

https://doi.org/10.1021/acscentsci.1c01389
ACS Cent. Sci. 2022, 8, 615−626